Fast Frequency Control Scheme through Adaptive Virtual Inertia Emulation

Uros Markovic*, Zhongda Chu*, Petros Aristidou§, Gabriela Hug*

* EEH - Power Systems Laboratory, ETH Zurich, Physikstrasse 3, 8092 Zurich, Switzerland
§ School of Electronic and Electrical Engineering, University of Leeds, Leeds LS2 9JT, UK
Emails: {markovic, hug}@eeh.ee.ethz.ch, zhchu@student.ethz.ch, p.aristidou@leeds.ac.uk

Abstract—This paper presents a novel virtual inertia controller for converters in power systems with high share of renewable resources. By combining the analytical study of system dynamics and a Linear-Quadratic Regulator (LQR)-based optimization technique, the optimal state feedback gain is determined, adapting the emulated inertia constant according to the frequency disturbance in the system. The optimality is achieved through trade-off between the critical frequency limits and the required control effort, i.e. utilization of the internal energy storage. The proposed controller is integrated into a state-of-the-art converter control scheme and verified through EMT simulations. The results show a significant improvement in the frequency response compared to an open-loop system, while also preserving drastically more DC-side energy than a non-adaptive controller.

Index Terms—linear-quadratic regulator (LQR), virtual inertia emulation, voltage source converter, adaptive controller

I. Introduction

The power system inertia provided by the rotating masses of large synchronous generators reduces as the penetration of renewable energy sources, usually coupled to the grid through fast-acting power inverters, increases [1], [2]. The loss of rotational inertia can have devastating effects on system dynamics, with large frequency deviations potentially triggering undesirable events, such as load-shedding and large-scale blackouts [3]. However, this study also shows that grid-scale energy storage devices can be employed for providing fast frequency support in isolated systems with high share of renewables. A downside of this approach though is the noise from the introduced harmonics, limited life cycle and low round-trip efficiency of the respective storage units.

Another common control approach for grid-connected inverters is the synchronous machine emulation, which provides a virtual inertia equivalent and "slows down" the transient system dynamics [4]. While the sole design and implementation of virtual inertia is quite straightforward, it is usually based on the assumption that the generator can produce or absorb infinitely large power, whereas in reality it is limited by its DC-side capacitor [5]. Hence, a distributed virtual inertia approach through regulating the DC-link voltages of power

converters was presented in [6], where the DC-link capacitors are aggregated into an extremely large unit for frequency support. The proposed method is implemented via a basic proportional frequency controller which drastically improves the overall system frequency response. However, it is only tested on a simplistic system and does not take into account the overall control effort, i.e. the value of the stored energy used for frequency regulation.

The addition of a derivative control term for containing excessive frequency excursions has been suggested in several studies [7]–[9]. In [7], a Rate-of-Change-of-Frequency (Ro-CoF) measurement contributes as an input to the traditional droop-like primary frequency control of a wind turbine; [8] proposes a droop controller in the form of a heuristic Ro-CoF exponential function, while [9] suggests the respective measurement as an input for an optimization-based online-tuning of a virtual synchronous machine. Nonetheless, all of the aforementioned techniques focus solely on the overall frequency improvement and disregard the costs and energy resources required for such regulation.

The goal of this paper is to derive a virtual inertia controller that would adapt the inertia gain according to the optimal trade-off between the transient frequency regulation and the respective energy requirements. First, we analytically study the system dynamics under the state feedback control of inertia constant. Based on the analysis, we propose an LQR-based adaptive inertia method that incorporates both the cost of frequency violation and the required control effort. Subsequently, the developed controller is implemented on a single state-of-the-art converter model, and verified through EMT simulations.

The remainder of the paper is structured as follows. In Section II, the system dynamics are investigated, and the respective frequency metrics under state feedback control are analytically derived. Section III describes the LQR formulation and optimal controller parametrization. Section IV showcases the EMT simulation results, whereas Section V draws main conclusions and discusses the outlook of the study.

II. Adaptive Virtual Inertia Properties

A. System Dynamics

We consider a second-order system consisting of an emulated swing equation and the turbine governor dynamics:

$$M\dot{\omega} = -D\omega + q + \Delta P \qquad (1)$$

$$\tau \dot{q} = -r^{-1}\omega - q \qquad (2)$$

where M and D are the normalized inertia and damping constants, and ω is the frequency deviation; ΔP and q denote the active power balance, i.e. a change in the drawn electric power, and the variation of the mechanical turbine power, respectively, while r and τ represent the droop gain and time constant of the turbine dynamics. It should be noted that the equations (1)-(2) are expressed in per-unit, and the ΔP term is considered as a known system disturbance. In steady state, the following holds:

$$\omega_{ss} = \frac{\Delta P}{D + r^{-1}} \quad , \quad q_{ss} = -r^{-1}\omega_{ss} \qquad (3)$$

From (1) and (2) we get the second-order differential equation of ω:

$$\ddot{\omega} = -(\frac{D}{M} + \frac{1}{\tau})\dot{\omega} - (\frac{1}{r\tau M} + \frac{D}{\tau M})\omega + \frac{\Delta P}{\tau M} + \frac{\Delta \dot{P}}{M} \qquad (4)$$
$$= -a\dot{\omega} - b\omega + c\Delta P + c\tau\Delta\dot{P}$$

where $a = \frac{D}{M} + \frac{1}{\tau}$, $b = \frac{1}{\tau M}(\frac{1}{r} + D)$ and $c = \frac{1}{\tau M}$. In Laplace s-domain the respective transfer function can be expressed as follows:

$$H(s) = \frac{\omega(s)}{\Delta P(s)} = \frac{c}{s^2 + as + b} + \frac{c\tau s}{s^2 + as + b} \qquad (5)$$

with the characteristic equation $s^2 + as + b = 0$, and the damping factor

$$\zeta = \frac{a}{2\sqrt{b}} = \frac{r^{\frac{1}{2}}(M + D\tau)}{2(M\tau + M\tau Dr)^{\frac{1}{2}}} \qquad (6)$$

We assume the system to be underdamped, $0 < \zeta < 1$, which results in the following inequality:

$$rM^2 - (2\tau Dr + 4\tau)M + r\tau^2 D^2 < 0 \qquad (7)$$

In order to obtain a time domain expression of ω, we consider ΔP to be a step change in the active power balance, i.e. a step disturbance $\Delta P(s) = s^{-1}$ in s-domain. Hence, a respective time domain solution of (4) can be computed through the inverse Laplace transform of the following frequency response:

$$\omega(s) = H(s)\Delta P(s) = \frac{c/s}{s^2 + as + b} + \frac{c\tau}{s^2 + as + b} \qquad (8)$$
$$= \omega_0(s) + s\tau\omega_0(s)$$

Therefore, by introducing the notation $\omega_n = \sqrt{b}$ and $\theta = \cos^{-1}\zeta$, in time domain we obtain

$$\omega(t) = \mathcal{L}^{-1}(\omega(s)) = \omega_0(t) + \tau\dot{\omega}_0(t) \qquad (9)$$

where $\omega_0(t)$ and $\dot{\omega}_0(t)$ are given by:

$$\omega_0(t) = \omega_{ss}(1 - \frac{1}{\sin\theta}e^{-\cos\theta\omega_n t}\sin((\omega_n\sin\theta)t + \theta)) \qquad (10)$$

$$\dot{\omega}_0(t) = \frac{\omega_{ss}\omega_n}{\sin\theta}e^{-\cos\theta\omega_n t}\sin((\omega_n\sin\theta)t) \qquad (11)$$

Since $0 < \zeta < 1$, the angle θ is bounded by $\theta \in (0, \frac{\pi}{2})$. Finally, adding up (10) and (11) yields

$$\omega(t) = \omega_{ss}(1 - \frac{1}{\sin\phi}e^{-\cos\theta\omega_n t}\sin(\omega_n\sin\theta t + \phi)) \qquad (12)$$

with ϕ satisfying the following conditions:

$$\cos\phi = \frac{\cos\theta - \tau\omega_n}{\beta} \qquad (13)$$

$$\sin\phi = \frac{\sin\theta}{\beta} \qquad (14)$$

In (13)-(14) we define $\beta = \sqrt{(\cos\theta - \tau\omega_n)^2 + \sin^2\theta}$. It can be shown that $\phi \in (\theta, \pi)$.

Proof. Having in mind that $\tau > 0$, let us observe the following expression:

$$\frac{d(\cos\phi)}{d\tau} = \frac{-\omega_n\beta + \omega_n\beta^{-1}(\cos\theta - \tau\omega_n)^2}{\beta^2}$$
$$= \frac{\omega_n}{\beta^3}((\cos\theta - \tau\omega_n)^2 - \beta^2) \qquad (15)$$
$$= \frac{\omega_n}{\beta^3}(-\sin^2\theta) < 0$$

Since $\cos\phi$ is continuous on τ, the respective boundaries are determined as

$$-1 = \lim_{\tau \to +\infty}\cos\phi(\tau) < \cos\phi(\tau) < \lim_{\tau \to 0}\cos\phi(\tau) = \cos\theta$$

which implies $\phi \in (\theta, \pi)$. ∎

Having derived a mathematical formulation of frequency response in time domain, we can now investigate the nadir and maximum RoCoF in the open-loop by taking the first and second derivative of $\omega(t)$ with respect to time:

$$\dot{\omega}(t) = \frac{\omega_{ss}\omega_n}{\sin\phi}e^{-\cos\theta\omega_n t}\sin((\omega_n\sin\theta)t + \phi - \theta) \qquad (16)$$

$$\ddot{\omega}(t) = -\frac{\omega_{ss}\omega_n^2}{\sin\phi}e^{-\zeta\omega_n t}\sin((\omega_n\sin\theta)t + \phi - 2\theta) \qquad (17)$$

The properties of frequency nadir are obtained from (16) by observing $\dot{\omega}(t_p) = 0$, which results in:

$$t_p = \frac{\pi + \theta - \phi}{\omega_n\sin\theta} \qquad (18)$$

$$\omega_{max} = \omega(t_p) = \omega_{ss}(1 + \frac{\sin\theta}{\sin\phi}e^{-\frac{\zeta(\pi+\theta-\phi)}{\sin\theta}}) \qquad (19)$$

Similarly, the maximum RoCoF can be investigated by setting $\ddot{\omega}(t_m) = 0$ in (17). However, the analysis is more complicated and yields the following two solutions, depending on the relationship between ϕ and θ:

$$|\dot{\omega}_{max}| = \begin{cases} \tau|\omega_{ss}|\omega_n^2 \equiv \frac{|\Delta P|}{M}, & \phi \in [2\theta, \pi) \\ |\omega_{ss}|\omega_n\frac{\sin\theta}{\sin\phi}e^{-\frac{\cos\theta(2\theta-\phi)}{\sin\theta}}, & \phi \in (\theta, 2\theta) \end{cases} \qquad (20)$$

whereas the time instance of occurrence is defined as:

$$t_m = \begin{cases} 0, & \phi \in [2\theta, \pi) \\ \frac{2\theta-\phi}{\omega_n\sin\theta}, & \phi \in (\theta, 2\theta) \end{cases} \qquad (21)$$

Proof. Let us first observe the case $\phi \in [2\theta, \pi)$, i.e. $\tau \in [\frac{1}{2\zeta\omega_n}, +\infty)$. From (17) we derive:

$$t_m = \frac{2\theta - \phi + \pi}{\omega_n \sin\theta} \tag{22}$$

$$\dot{\omega}(t_m) = -\omega_{ss}\omega_n \frac{\sin\theta}{\sin\phi} e^{-\frac{\zeta(2\theta - \phi + \pi)}{\sin\theta}} \tag{23}$$

However, due to the exponential decay nature of $\dot{\omega}(t)$, we need to compare $\dot{\omega}(t_m)$ against $\dot{\omega}(0)$ in order to determine $\dot{\omega}_{\max}$:

$$|\dot{\omega}(0)| = \frac{|\omega_{ss}|\omega_n \sin(\phi - \theta)}{\sin\phi}$$
$$> \frac{|\omega_{ss}|\omega_n \sin\theta}{\sin\phi} e^{-\zeta\omega_n t_m} = |\dot{\omega}(t_m)| \tag{24}$$

Therefore:

$$|\dot{\omega}_{\max}| = |\dot{\omega}(0)| = \tau|\omega_{ss}|\omega_n^2 = \frac{|\Delta P|}{M} \tag{25}$$

Now the assumption is $\phi \in (\theta, 2\theta)$, i.e. $\tau \in (0, \frac{1}{2\zeta\omega_n})$. This leads to the following expression for t_m:

$$t_m = \frac{2\theta - \phi}{\omega_n \sin\theta} \tag{26}$$

Again, we have to compare $\dot{\omega}(t_m)$ and $\dot{\omega}(0)$:

$$|\dot{\omega}(0)| = \frac{|\omega_{ss}|\omega_n \sin(\phi - \theta)}{\sin\phi} \tag{27}$$

$$|\dot{\omega}(t_m)| = \frac{|\omega_{ss}|\omega_n \sin\theta}{\sin\phi} e^{-\frac{\cos\theta(2\theta - \phi)}{\sin\theta}} \tag{28}$$

which, due to the fact that $|\omega_{ss}|$, ω_n and $\sin\phi$ are positive, is equivalent to analyzing the expressions:

$$h_1(\phi) = \sin(\phi - \theta) \tag{29}$$
$$h_2(\phi) = \sin\theta \, e^{-\frac{\cos\theta(2\theta - \phi)}{\sin\theta}} \tag{30}$$

Let us observe the nature and boundaries of h_1 and h_2:

$$h_1(\theta) = 0 < \sin\theta \, e^{-\cos\theta} = h_2(\theta)$$
$$h_1(2\theta) = \sin\theta = h_2(2\theta) \tag{31}$$
$$\frac{d(h_2(\phi) - h_1(\phi))}{d\phi} = \cos\theta \, e^{-\frac{\cos\theta(2\theta - \phi)}{\sin\theta}} - \cos(\phi - \theta)$$

Since the last term in (31) is negative, it can be concluded that $h_1(\phi) < h_2(\phi), \forall\phi \in (\theta, 2\theta)$, which further indicates $|\dot{\omega}(0)| < |\dot{\omega}(t_m)|$. Finally, we derive:

$$|\dot{\omega}_{\max}| = |\dot{\omega}(t_m)| = |\omega_{ss}|\omega_n \frac{\sin\theta}{\sin\phi} e^{-\frac{\cos\theta(2\theta - \phi)}{\sin\theta}} \tag{32}$$

∎

The respective frequency response properties from (18)-(19) are depicted in Fig. 1. It is shown in (19) that the value of ϕ determines the RoCoF characteristic of the system. However, this can be simplified by combining the expression for a, ω_n and ζ as follows:

$$\phi \geq 2\theta \iff \tau \geq \frac{1}{2\zeta\omega_n}$$
$$\iff \tau \geq \frac{1}{a} \iff \frac{1}{\tau} \leq a \iff \frac{1}{\tau} \leq \frac{D}{M} + \frac{1}{\tau} \tag{33}$$
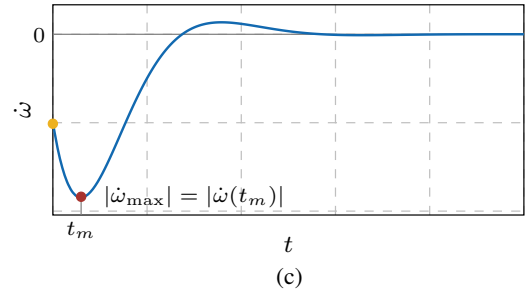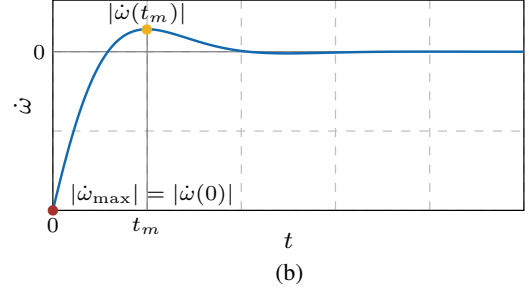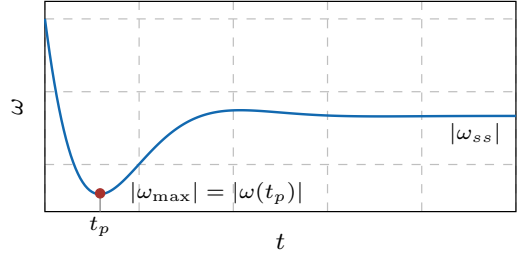
Fig. 1: Frequency response characteristic of the second-order system: (a) frequency nadir; (b) maximum RoCoF for $\phi \in [2\theta, \pi)$; (c) maximum RoCoF for $\phi \in (\theta, 2\theta)$;

which indicates that $\phi \in [2\theta, \pi)$, $\forall D, M > 0$. Hence, the maximum RoCoF of the investigated second-order system occurs always at $t = 0$, and is determined simply by the active power disturbance and provided inertia. This implies that regulating inertia adaptively in the closed-loop could have significant improvements on the overall frequency response.

B. Linearization and Closed-Loop Analysis

If we consider a constant step change disturbance $\Delta P \, \forall t \in [0^+, +\infty)$, then (4) is transformed into:

$$\ddot{\omega} = -(\frac{D}{M} + \frac{1}{\tau})\dot{\omega} - (\frac{1}{r\tau M} + \frac{D}{\tau M})\omega + \frac{\Delta P}{\tau M}$$
$$= -a\dot{\omega} - b\omega + c\Delta P \tag{34}$$

Defining the state-space and control input as $x = \begin{bmatrix} \omega & \dot{\omega} \end{bmatrix}^T$ and $u = M$, respectively, (34) can be rewritten as follows:

$$\begin{bmatrix} \dot{\omega} \\ \ddot{\omega} \end{bmatrix} = \begin{bmatrix} 0 & I \\ -(\frac{1}{r\tau M} + \frac{D}{\tau M}) & -(\frac{D}{M} + \frac{1}{\tau}) \end{bmatrix} \begin{bmatrix} \omega \\ \dot{\omega} \end{bmatrix} + \begin{bmatrix} 0 \\ \frac{\Delta P}{\tau M} \end{bmatrix} \tag{35}$$

with the initial condition $x(0) = \begin{bmatrix} 0 & \dot{\omega}(0^+) \end{bmatrix}^T$.

Let us now linearize the system in (35) around its post-disturbance steady-state equilibrium point (x_0, u_0), where $x_0 = \left[\frac{\Delta P}{D + r^{-1}} \quad 0\right]^T$ and $u_0 = M_0$:

$$\begin{bmatrix} \dot{\omega} \\ \ddot{\omega} \end{bmatrix} = \underbrace{\begin{bmatrix} 0 & 1 \\ -(\frac{1}{r\tau M_0} + \frac{D}{\tau M_0}) & -(\frac{D}{M_0} + \frac{1}{\tau}) \end{bmatrix}}_{A} \begin{bmatrix} \omega \\ \dot{\omega} \end{bmatrix} + \underbrace{\begin{bmatrix} 0 \\ \frac{-\Delta P}{\tau M_0^2} \end{bmatrix}}_{B} \Delta M$$

$$= \begin{bmatrix} 0 & 1 \\ -b^* & -a^* \end{bmatrix} \begin{bmatrix} \omega \\ \dot{\omega} \end{bmatrix} + \begin{bmatrix} 0 \\ g \end{bmatrix} \Delta M \qquad (36)$$

Introducing the following state feedback control input depicted in Fig. 2:

$$\Delta u = \Delta M = M - M_0 = -Kx = -\begin{bmatrix} K_1 & K_2 \end{bmatrix} \begin{bmatrix} \omega \\ \dot{\omega} \end{bmatrix} \qquad (37)$$

results in the closed-loop system of the form $\dot{x} = \mathcal{A}x$, with the semi-simple matrix $\mathcal{A}$ defined as

$$\mathcal{A} = \begin{bmatrix} 0 & 1 \\ -(\frac{1}{r\tau M_0} + \frac{D}{\tau M_0} - \frac{\Delta P K_1}{\tau M_0^2}) & -(\frac{D}{M_0} + \frac{1}{\tau} - \frac{\Delta P K_2}{\tau M_0^2}) \end{bmatrix}$$

$$= \begin{bmatrix} 0 & 1 \\ -b^* - gK_1 & -a^* - gK_2 \end{bmatrix} \qquad (38)$$

In order to find the solution to the aforementioned LTI system, we diagonalize $\mathcal{A}$ as follows:

$$\mathcal{A} = \begin{bmatrix} 1 & 1 \\ \lambda_1 & \lambda_2 \end{bmatrix} \begin{bmatrix} \lambda_1 & 0 \\ 0 & \lambda_2 \end{bmatrix} \begin{bmatrix} 1 & 1 \\ \lambda_1 & \lambda_2 \end{bmatrix}^{-1} \qquad (39)$$

where λ_1 and λ_2 are the eigenvalues of $\mathcal{A}$ satisfying:

$$\lambda^2 + (a^* + gK_2)\lambda + (b^* + gK_1) = 0 \qquad (40)$$

Therefore, the time-domain solution to the linearized closed-loop system is given by $x(t) = e^{\mathcal{A}t}x(0)$, i.e.

$$\begin{bmatrix} \omega(t) \\ \dot{\omega}(t) \end{bmatrix} = \begin{bmatrix} 1 & 1 \\ \lambda_1 & \lambda_2 \end{bmatrix} \begin{bmatrix} e^{\lambda_1 t} & 0 \\ 0 & e^{\lambda_2 t} \end{bmatrix} \begin{bmatrix} 1 & 1 \\ \lambda_1 & \lambda_2 \end{bmatrix}^{-1} \begin{bmatrix} \omega(0) \\ \dot{\omega}(0) \end{bmatrix}$$

$$= \frac{\dot{\omega}(0)}{\lambda_2 - \lambda_1} \begin{bmatrix} -e^{\lambda_1 t} + e^{\lambda_2 t} \\ -\lambda_1 e^{\lambda_1 t} + \lambda_2 e^{\lambda_2 t} \end{bmatrix}, \forall \lambda_1 \neq \lambda_2 \qquad (41)$$

For the case where $\lambda_1 = \lambda_2$, the above solution needs to be modified by the Jordan normal form of matrix $\mathcal{A}$ instead of diagonalization. However, we could always put the two eigenvalues at different positions by turning the feedback gains. Setting $\dot{\omega}(t_p) = 0$ yields the frequency nadir properties:

$$t_p = \frac{\ln(\lambda_1/\lambda_2)}{\lambda_2 - \lambda_1} \qquad (42)$$

$$\omega_{\max} = \omega(t_p) = \dot{\omega}(0)\frac{e^{\lambda_2 t_p} - e^{\lambda_1 t_p}}{\lambda_2 - \lambda_1} \qquad (43)$$

Similarly, observing the expression $\ddot{\omega}(t_m) = 0$ yields:

$$t_m = \frac{\ln(\lambda_1^2/\lambda_2^2)}{\lambda_2 - \lambda_1} \qquad (44)$$

$$\dot{\omega}(t_m) = \dot{\omega}(0)\underbrace{\frac{\lambda_2 e^{\lambda_2 t_m} - \lambda_1 e^{\lambda_1 t_m}}{\lambda_2 - \lambda_1}}_{K_\lambda} \qquad (45)$$
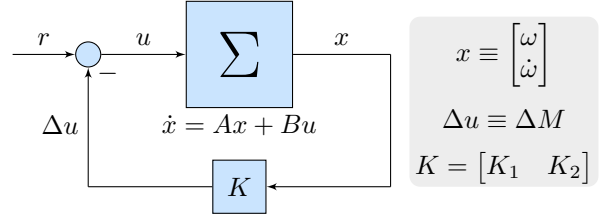
Fig. 2: State feedback control of adaptive virtual inertia.

It can be shown that $-1 < K_\lambda < 1$, which indicates that the maximum RoCoF of the closed-loop system would also occur at $t = 0$, i.e. $\dot{\omega}_{\max} = \dot{\omega}(0)$.

Proof. We observe two different cases, depending on the nature of the eigenvalues λ_1 and λ_2:

Case 1: Matrix $\mathcal{A}$ has two negative real eigenvalues and w.l.o.g. we assume $\lambda_1 < \lambda_2 < 0$. Since $t_m > 0 \implies e^{\lambda_2 t_m} > e^{\lambda_1 t_m}$, which implies $\lambda_2 e^{\lambda_2 t_m} < \lambda_2 e^{\lambda_1 t_m}$, and furthermore:

$$\underbrace{\frac{\lambda_2 e^{\lambda_2 t_m} - \lambda_1 e^{\lambda_1 t_m}}{\lambda_2 - \lambda_1}}_{K_\lambda} < \underbrace{\frac{\lambda_2 e^{\lambda_1 t_m} - \lambda_1 e^{\lambda_1 t_m}}{\lambda_2 - \lambda_1}}_{e^{\lambda_1 t_m}} < 1 \qquad (46)$$

Secondly, $-1 < K_\lambda$ is equivalent to the following statement:

$$-1 < K_\lambda \iff \lambda_1 - \lambda_2 < \lambda_2 e^{\lambda_2 t_m} - \lambda_1 e^{\lambda_1 t_m}$$
$$\iff \lambda_1 + \lambda_1 e^{\lambda_1 t_m} < \lambda_2 + \lambda_2 e^{\lambda_2 t_m} \qquad (47)$$
$$\iff f(\lambda_1) < f(\lambda_2)$$

where $f(\lambda) = \lambda + \lambda e^{\lambda t_m}$ is a strictly increasing function $\forall \lambda < 0$, which further implies:

$$\frac{df(\lambda)}{d\lambda} = 1 + (1 + \lambda t_m)e^{\lambda t_m} > 0 \qquad (48)$$

Since $\ddot{f}(\lambda) = 0 \iff t_m e^{\lambda t_m}(2 + \lambda t_m) = 0$, we can compute $\min(\dot{f}(\lambda)) = \dot{f}(-2t_m^{-1}) = 1 - e^{-2} > 0$. Therefore, $\dot{f}(\lambda) > 0, \forall \lambda < 0$, which confirms the statement in (48) and proves that $-1 < K_\lambda$.

Case 2: The eigenvalues of $\mathcal{A}$ are a pair of complex conjugates and w.l.o.g. we assume $\lambda_1 = \alpha + j\beta_1 = ce^{j\theta_1}$ and $\lambda_2 = \alpha + j\beta_2 = ce^{j\theta_2}$, with $\alpha < 0, \beta_1 = -\beta_2 > 0, c > 0$ and $\theta_1 = -\theta_2 \in (\frac{\pi}{2}, \pi)$. Hence, K_λ can be expressed as follows:

$$K_\lambda = \frac{\lambda_2 e^{\lambda_2 t_m} - \lambda_1 e^{\lambda_1 t_m}}{\lambda_2 - \lambda_1}$$
$$= \frac{ce^{\alpha t_m}(e^{j(\theta_2 + \beta_2 t_m)} - e^{-j(\theta_2 + \beta_2 t_m)})}{2j\beta_2} \qquad (49)$$
$$= \frac{ce^{\alpha t_m}\sin(\theta_2 + \beta_2 t_m)}{\beta_2}$$

while t_m can also be simplified accordingly:

$$t_m = \frac{\ln\frac{\lambda_1^2}{\lambda_2^2}}{\lambda_2 - \lambda_1} = \frac{\theta_1 - \theta_2 + 2k\pi}{\beta_2}, \quad k \in \mathbb{Z} \qquad (50)$$

Therefore, the first peak value of $\dot{\omega}(t)$ for $t \in [0, +\infty)$ is attained at $k = 1$. Substituting the respective value of t_m in (49) yields:

$$K_\lambda = \frac{e^{\alpha t_m}\sin\theta_1}{\beta_2/c} = \frac{e^{\alpha t_m}\sin\theta_1}{\sin(\theta_1 - \pi)} = -e^{\alpha t_m} \in (-1, 0) \qquad (51)$$

which concludes the proof. ∎

Finally, combining (25) and (37) results in:

$$\dot{\omega}_{\max} = \frac{\Delta P}{M(0)} = \frac{\Delta P}{M_0 - K_2 \dot{\omega}_{\max}} \qquad (52)$$

Hence, the maximum RoCoF of the closed-loop system is solely dependent on the active power disturbance, equilibrium virtual inertia and the RoCoF feedback gain of our controller, as follows:

$$\dot{\omega}_{\max} = \frac{M_0 - (M_0^2 - 4K_2\Delta P)^{\frac{1}{2}}}{2K_2} \qquad (53)$$

III. LQR-Based Controller Design

A. Optimization Problem

Having derived a mathematical model of the inertia emulation controller, we focus on tuning it. The goal is to obtain feedback gains (K_1, K_2) such that the converter provides an optimal contribution to frequency regulation, while also considering the "costs" of DC-side utilization. In order to achieve such trade-off, a following optimization problem is proposed:

$$\min_{\omega, \dot{\omega}, \Delta M} \int_0^\infty \left(\omega^T Q_1 \omega + \dot{\omega}^T Q_2 \dot{\omega} + \Delta M^T R \Delta M \right) dt \quad (54a)$$

$$\text{s.t} \qquad \begin{bmatrix} \dot{\omega} \\ \ddot{\omega} \end{bmatrix} = A \begin{bmatrix} \omega \\ \dot{\omega} \end{bmatrix} + B \Delta M \qquad (54b)$$

$$\Delta M = - \underbrace{\begin{bmatrix} K_1 & K_2 \end{bmatrix}}_{K} \begin{bmatrix} \omega \\ \dot{\omega} \end{bmatrix} \qquad (54c)$$

which penalizes three quadratic objectives: frequency deviation from nominal (ω), RoCoF ($\dot{\omega}$), and control effort (Δu), which correlates to the amount of additionally provided virtual inertia (ΔM); Q_1, Q_2 and R denote the respective penalty factors. The optimization constraints (54b)-(54c) are defined through linearized system dynamics described in Section II-B.

The presented formulation in (54) represents a Linear-Quadratic Regulator (LQR). Therefore, one can obtain the optimal control feedback gain that minimizes the objective function in (54a) as $K^* = R^{-1}B^T P$, where P is the solution of the following algebraic Riccati equation:

$$A^T P + PA - PBR^{-1}B^T P + Q = 0 \qquad (55)$$

and $Q = diag(Q_1, Q_2)$. The expression in (55) implies that the selection of cost factors Q and R completely determines the optimal controller gain, thus highlighting the importance of the controller parametrization discussed in the subsequent section.

B. Parametrization and Implementation

One of the most common (initial) LQR tuning approaches is to consider all objective costs equally [10], i.e. to select the respective weights such that $J_1 = J_2 = J_3$:

$$J_1 = Q_1 x_{\max}^2 \equiv Q_1 (\omega_{\max})^2 \qquad (56)$$

$$J_2 = Q_2 \dot{x}_{\max}^2 \equiv Q_2 (\dot{\omega}_{\max})^2 \qquad (57)$$

$$J_3 = R \Delta u_{\max}^2 \equiv R (\Delta M_{\max})^2 \qquad (58)$$

TABLE I: Controller Parameters

Parameter	Symbol	Value
Nominal frequency	f_n	50 Hz
LPF cut-off frequency	f_c	25 Hz
Active droop gain	r	0.04 p.u.
Inertia constant	M_0	1 s
Damping constant	D	50 p.u.
Turbine time constant	τ	3 s

This is usually achieved by fixing one penalty factor, e.g. $R = 1$ in our case, and adjusting the remaining ones accordingly:

$$Q_1 = R \left(\frac{\Delta M_{\max}}{\omega_{\max}} \right)^2 \qquad (59)$$

$$Q_2 = R \left(\frac{\Delta M_{\max}}{\dot{\omega}_{\max}} \right)^2 \qquad (60)$$

The ENTSO-E report on frequency stability evaluation criteria for low inertia systems [11] states the following limits for both ordinary and exceptional contingencies: $f \in [49.8, 50.2]$ Hz; $|df/dt| \in [0, 2]$ Hz/s. Hence, the corresponding LQR thresholds are set to $\omega_{\max} = 0.004$ p.u. and $\dot{\omega}_{\max} = 0.04$ p.u. Furthermore, we make an assumption that the respective frequency excursions correlate to a virtual inertia increase of 50%, i.e. $\Delta M_{\max} = 0.5 M_0$. The employed controller model is obtained from the following equivalence between an emulated virtual inertia and a standard droop control [12]:

$$M_0 = \frac{1}{r f_c} \quad , \quad D = \frac{1}{r} \qquad (61)$$

where f_c denotes a low-pass filter cut-off frequency. All parameters are given in Table I, whereas the implemented control block structure is depicted in Fig. 3. It showcases the *plug'n'play* properties of the adaptive controller, as it can easily be adopted into an existing virtual inertia structure, e.g. a virtual synchronous machine control of doubly-fed induction generators. It should be noted that the adaptive inertia constant gain in Fig. 3 is of the form $M = M_0 + \Delta M$.

IV. Results

In order to qualitatively verify the proposed adaptive approach, the virtual inertia controller has been incorporated into
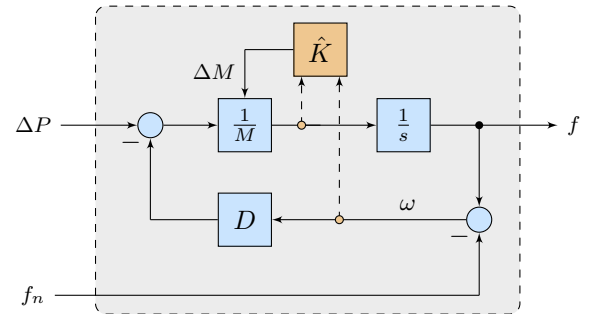
Fig. 3: Proposed virtual inertia control design ($\hat{K} = -K$); the components of the adaptive controller are colored differently.

a state-of-the-art converter control scheme [13]. The modeling and EMT simulations have been conducted in MATLAB Simulink and Simscape Power Systems platforms, with a focus on an islanded inverter unit supplying a purely resistive load. We investigate the system frequency response under a sudden step-change of 20% in the active load power, interpreted as $\Delta P = -0.2$ p.u. in (1).

For the purpose of this study, three different control techniques have been employed: (i) a traditional virtual inertia model with a constant inertia term ($M_1 = M_0$); (ii) an LQR-based adaptive inertia controller ($M_2 = M_0 + \Delta M$); and (iii) a non-adaptive controller that changes inertia constant in a step-wise fashion at the instance of load change; the amount of provided inertia should vary between the maximum values of the previous two controllers, i.e. $M_3^{\min} = M_0$ and $M_3^{\max} = M_2^{\max}$.

The results shown in Fig. 4a indicate that the feedback control greatly improves the frequency response, as both adaptive and non-adaptive approach significantly reduce the frequency nadir ($\approx 10\%$). Due to an explicit step function and immediate deployment of additional inertia, the frequency excursion in case of a non-adaptive controller is slightly lower than for the LQR-based model. However, it is achieved at the cost of overall slower system dynamics, which leads to an increase in steady-state convergence time. This implies that the higher inertia is needed only within a very short window around the instance of fault occurrence. Furthermore, another downside of a non-adaptive approach is a drastically higher DC-side energy consumption, as depicted in Fig. 4b.

(a)

(b)
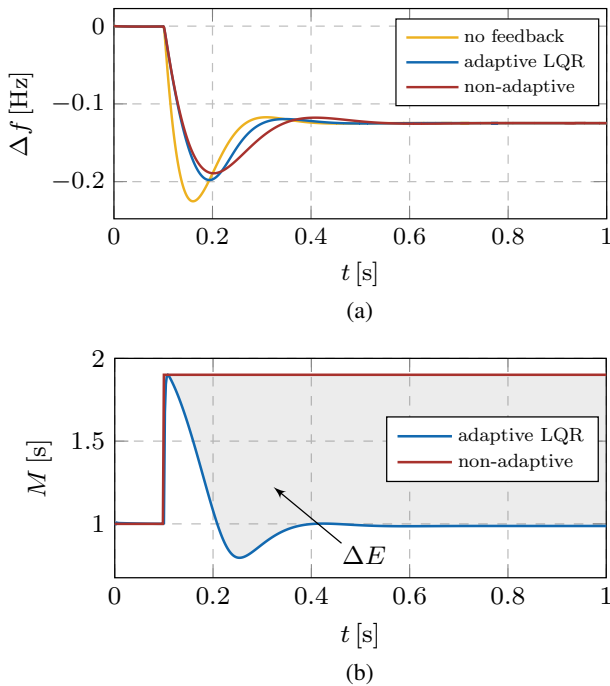
Fig. 4: System response under different virtual inertia controllers: (a) frequency deviation; (b) emulated inertia constant.

V. CONCLUSION

This paper introduces a novel distributed virtual inertia concept for converters in power systems with high share of renewable resources. The system dynamics under such control design have been thoroughly investigated, and analytic formulation of frequency and RoCoF in time domain were derived. Subsequently, the expressions for frequency nadir and maximum RoCoF were obtained, proving an explicit impact of the proposed controller on the respective system metrics.

An LQR-based optimal feedback controller was proposed to adaptively adjust the emulated inertia constant according to the frequency disturbance in the system, while simultaneously preserving a trade-off between the critical frequency limits and the required control effort. The proposed approach was incorporated into a detailed state-of-the-art control scheme and verified on an individual converter unit. The simulation results show a drastic improvement in frequency response compared to an open-loop system, while also preserving significantly more DC-side energy than a non-adaptive controller. The future work will focus on the impact of adaptive damping control, the analysis of optimal LQR cost factors, as well as the extension into a multi-inverter case.

REFERENCES

[1] F. Blaabjerg, R. Teodorescu, M. Liserre, and A. V. Timbus, "Overview of control and grid synchronization for distributed power generation systems," *IEEE Transactions on Industrial Electronics*, vol. 53, no. 5, pp. 1398–1409, Oct 2006.

[2] J. M. Carrasco *et al.*, "Power-electronic systems for the grid integration of renewable energy sources: A survey," *IEEE Transactions on Industrial Electronics*, vol. 53, no. 4, pp. 1002–1016, June 2006.

[3] G. Delille, B. Francois, and G. Malarange, "Dynamic frequency control support by energy storage to reduce the impact of wind and solar generation on isolated power system's inertia," *IEEE Transactions on Sustainable Energy*, vol. 3, no. 4, pp. 931–939, Oct 2012.

[4] Q. C. Zhong and G. Weiss, "Synchronverters: Inverters that mimic synchronous generators," *IEEE Transactions on Industrial Electronics*, vol. 58, no. 4, pp. 1259–1267, April 2011.

[5] M. Ashabani and Y. A. R. I. Mohamed, "Novel comprehensive control framework for incorporating vscs to smart power grids using bidirectional synchronous-vsc," *IEEE Transactions on Power Systems*, vol. 29, no. 2, pp. 943–957, March 2014.

[6] J. Fang, X. Li, and Y. Tang, "Grid-connected power converters with distributed virtual power system inertia," in *2017 IEEE Energy Conversion Congress and Exposition (ECCE)*, Oct 2017, pp. 4267–4273.

[7] J. Morren, S. W. H. de Haan, W. L. Kling, and J. A. Ferreira, "Wind turbines emulating inertia and supporting primary frequency control," *IEEE Transactions on Power Systems*, vol. 21, no. 1, pp. 433–434, Feb 2006.

[8] N. Soni, S. Doolla, and M. C. Chandorkar, "Improvement of transient response in microgrids using virtual inertia," *IEEE Transactions on Power Delivery*, vol. 28, no. 3, pp. 1830–1838, July 2013.

[9] M. A. T. L., L. A. C. Lopes, L. A. M. T., and J. R. E. C., "Self-tuning virtual synchronous machine: A control strategy for energy storage systems to support dynamic frequency control," *IEEE Transactions on Energy Conversion*, vol. 29, no. 4, pp. 833–840, Dec 2014.

[10] S. Chandrapati, *Design and Implementation: Linear Quadratic Regulator*. LAP LAMBERT Academic Publishing, 2011.

[11] "Frequency stability evaluation criteria for the synchronous zone of continental europe," ENTSO-E, Tech. Rep., 2016.

[12] R. Ofir, U. Markovic, P. Aristidou, and G.Hug, "Droop vs. virtual inertia: Comparison from the perspective of converter operation mode," in *2018 IEEE International Energy Conference (ENERGYCON)*, June 2018.

[13] U. Markovic, O. Stanojev, P. Aristidou, and G. Hug, "Partial grid forming concept for 100% inverter-based transmission systems," in *2018 IEEE Power and Energy Society General Meeting (PESGM)*, Aug 2018.